AFRL-RQ-WP-TP-2015-0055

SOL-GEL-DERIVED LITHIUM SUPERIONIC CONDUCTOR $LI_{1.5}AL_{0.5}GE_{1.5}(PO_4)_3$ ELECTROLYTE FOR SOLID-STATE LITHIUM-OXYGEN BATTERIES (POSTPRINT)

Padmakar Kichambare and Stanley Rodrigues

Electrical Systems Branch
Power and Control Division

Thomas Howell

GE Aviation

MARCH 2014

AIR FORCE RESEARCH LABORATORY
AEROSPACE SYSTEMS DIRECTORATE
WRIGHT-PATTERSON AIR FORCE BASE, OH 45433-7541
AIR FORCE MATERIEL COMMAND
UNITED STATES AIR FORCE

NOTICE AND SIGNATURE PAGE

Using Government drawings, specifications, or other data included in this document for any purpose other than Government procurement does not in any way obligate the U.S. Government. The fact that the Government formulated or supplied the drawings, specifications, or other data does not license the holder or any other person or corporation; or convey any rights or permission to manufacture, use, or sell any patented invention that may relate to them.

This report was cleared for public release by the USAF 88th Air Base Wing (88 ABW) Public Affairs Office (PAO) and is available to the general public, including foreign nationals.

Copies may be obtained from the Defense Technical Information Center (DTIC) (http://www.dtic.mil).

AFRL-RQ-WP-TP-2015-0055 HAS BEEN REVIEWED AND IS APPROVED FOR PUBLICATION IN ACCORDANCE WITH ASSIGNED DISTRIBUTION STATEMENT.

*//Signature//
STANLEY J. RODRIGUES
Project Manager
Electrical Systems Branch
Power and Control Division

//Signature//
GREGORY L. FRONISTA, Chief
Electrical Systems Branch
Power and Control Division
Aerospace Systems Directorate

//Signature//
DANIEL B. THOMPSON
Acting Division Chief
Power and Control Division
Aerospace Systems Directorate

This report is published in the interest of scientific and technical information exchange, and its publication does not constitute the Government's approval or disapproval of its ideas or findings.

*Disseminated copies will show "//Signature//" stamped or typed above the signature blocks.

REPORT DOCUMENTATION PAGE

Form Approved
OMB No. 0704-0188

1. REPORT DATE *(DD-MM-YY)*	2. REPORT TYPE	3. DATES COVERED *(From - To)*
March 2014	Journal Article Postprint	01 March 2014 – 01 March 2014

4. TITLE AND SUBTITLE
SOL-GEL-DERIVED LITHIUM SUPERIONIC CONDUCTOR $LI_{1.5}AL_{0.5}GE_{1.5}(PO_4)_3$ ELECTROLYTE FOR SOLID-STATE LITHIUM-OXYGEN BATTERIES (POSTPRINT)

5a. CONTRACT NUMBER
In-house

5b. GRANT NUMBER

5c. PROGRAM ELEMENT NUMBER
62203F

6. AUTHOR(S)
Padmakar Kichambare and Stanley Rodrigues (AFRL/RQQE)
Thomas Howell (GE Aviation)

5d. PROJECT NUMBER
3145

5e. TASK NUMBER
N/A

5f. WORK UNIT NUMBER
Q10H

7. PERFORMING ORGANIZATION NAME(S) AND ADDRESS(ES)

Electrical Systems Branch (AFRL/RQQE)
Power and Control Division, Air Force Research Laboratory
Aerospace Systems Directorate
Wright-Patterson Air Force Base, OH 45433-7541
Air Force Materiel Command, United States Air Force

GE Aviation
Cincinnati, OH 45215

8. PERFORMING ORGANIZATION REPORT NUMBER
AFRL-RQ-WP-TP-2015-0055

9. SPONSORING/MONITORING AGENCY NAME(S) AND ADDRESS(ES)
Air Force Research Laboratory
Aerospace Systems Directorate
Wright-Patterson Air Force Base, OH 45433-7541
Air Force Materiel Command
United States Air Force

10. SPONSORING/MONITORING AGENCY ACRONYM(S)
AFRL/RQQE

11. SPONSORING/MONITORING AGENCY REPORT NUMBER(S)
AFRL-RQ-WP-TP-2015-0055

12. DISTRIBUTION/AVAILABILITY STATEMENT
Approved for public release; distribution unlimited.

13. SUPPLEMENTARY NOTES
PA Case Number: 88ABW-2014-0180; Clearance Date: 22 Jan 2014.

Report published in *Energy Technology*, Vol. 2, 2014.

14. ABSTRACT
Lithium aluminum germanium phosphate (LAGP) is attracting a great deal of attention as a solid electrolyte for lithium-oxygen (Li-O_2) batteries due to its high ionic conductivity. In this study, LAGP is prepared by a sol-gel process using comparatively low-cost $GeCl_2$ as one of the reactants. The final product (LAGP) is obtained by sintering the dry precursor gel at 900 °C for 6 h. The influence of the duration of water evaporation during polymerization on the microstructure of LAGP has been examined. The structure, morphology, and electrochemical properties of LAGP are investigated by employing X-ray diffraction (XRD), scanning electron microscopy (SEM), nitrogen adsorption-desorption analysis, and electrochemical impedance spectroscopy. XRD studies confirm the formation of $Li_{1.5}Al_{0.5}Ge_{1.5}(PO_4)_3$ as a primary phase along with small amounts of $AlPO_4$ and Li_2O as impurity phases. LAGP specimens have ionic conductivities in the range of 10^{-4} to 10^{-5} Scm^{-1} at room temperature. In addition, LAGP also exhibits electrocatalytic activity towards the oxygen-reduction and evolution reactions. These results demonstrate the potential of LAGP prepared by sol-gel processes as a solid electrolyte for lithium-ion conduction in solid-state lithium-oxygen batteries.

15. SUBJECT TERMS
lithium-oxygen battery, oxygen reduction reactions, nitrogen-doped carbon, lithium aluminum germanium phosphate

16. SECURITY CLASSIFICATION OF:			17. LIMITATION OF ABSTRACT:	18. NUMBER OF PAGES	19a. NAME OF RESPONSIBLE PERSON (Monitor)
a. REPORT	b. ABSTRACT	c. THIS PAGE			Stanley J. Rodrigues
Unclassified	Unclassified	Unclassified	SAR	12	19b. TELEPHONE NUMBER *(Include Area Code)* N/A

DOI: 10.1002/ente.201300139

Sol–Gel-Derived Lithium Superionic Conductor $Li_{1.5}Al_{0.5}Ge_{1.5}(PO_4)_3$ Electrolyte for Solid-State Lithium–Oxygen Batteries

Padmakar D. Kichambare,*[a] Thomas Howell,[a, b] and Stanley Rodrigues[a]

Lithium aluminium germanium phosphate (LAGP) is attracting a great deal of attention as a solid electrolyte for lithium–oxygen ($Li–O_2$) batteries due to its high ionic conductivity. In this study, LAGP is prepared by a sol–gel process using comparatively low-cost $GeCl_2$ as one of the reactants. The final product (LAGP) is obtained by sintering the dry precursor gel at 900 °C for 6 h. The influence of the duration of water evaporation during polymerization on the microstructure of LAGP has been examined. The structure, morphology, and electrochemical properties of LAGP are investigated by employing X-ray diffraction (XRD), scanning electron microscopy (SEM), nitrogen adsorption–desorption analysis, and electrochemical impedance spectroscopy. XRD studies confirm the formation of $Li_{1.5}Al_{0.5}Ge_{1.5}(PO_4)_3$ as a primary phase along with small amounts of $AlPO_4$ and Li_2O as impurity phases. LAGP specimens have ionic conductivities in the range of 10^{-4} to 10^{-5} S cm^{-1} at room temperature. In addition, LAGP also exhibits electrocatalytic activity towards the oxygen-reduction and evolution reactions. These results demonstrate the potential of LAGP prepared by sol–gel processes as a solid electrolyte for lithium-ion conduction in solid-state lithium–oxygen batteries.

Introduction

Lithium–oxygen batteries are one of the most promising high-energy-density electrochemical power sources anticipated to impact future battery technologies.[1–5] This battery consists of lithium metal anode, lithium-ion-conducting electrolyte, and oxygen cathode. During cell discharge, oxygen is reduced at the cathode as the lithium metal is oxidized.[6] Lithium peroxide and/or lithium oxides[7–12] are formed as discharge products that are stored in voids of the cathode matrix. Upon charging, these discharge products are converted back to lithium and oxygen.[13–16] To realize a long-term operational stability of these batteries, a solid ceramic electrolyte with high ionic conductivity, wide electrochemical operating window, and good stability against chemical reactions with the cathode and anode materials is desired. Lithium superionic conductors are promising materials as electrolytes for solid-state lithium batteries due to their incombustibility characteristics for increased safety.[17,18]

Among lithium superionic conductors, lithium aluminum germanium phosphate (LAGP) and lithium aluminum titanium phosphate (LATP) are of importance for the development of solid-state lithium–oxygen batteries.[19–24] LATP and LAGP are derivatives of $LiTi_2(PO_4)_3$ and $LiGe_2(PO_4)_3$, respectively. Both LATP and LAGP consist of two polyhedral: MO_6 octahedra (M = Ti, Ge, etc.) and PO_4 tetrahedra, linked by their corners to form a rigid $[M_2(PO_4)_3]^-$ skeleton. The skeleton provides a three-dimensional array of tunnels through which the Li^+ can migrate. LAGP is of particular interest as it also helps to facilitate the reduction of oxygen in lithium–oxygen batteries.[25] In addition, LAGP can be made stable against reaction with Li metal.[19,20,26] Synthesis of LAGP has been reported by various techniques such as melt quenching,[27,28] conventional solid-state sintering,[29] sol–gel,[30] and flame–spray methods.[31] High conductivities of 4.0×10^{-4} S cm^{-1}[27] and 5.08×10^{-3} S cm^{-1}[28] at room temperature were reported for LAGP prepared by using the melt-quenching method. Leo et al. reported a bulk conductivity of 3.99×10^{-4} S cm^{-1} for $Li_{1.4}Al_{0.4}Ge_{1.6}(PO_4)_3$[29] prepared by using a solid-state method. On the other hand, the bulk conductivities for $Li_{1.4}Al_{0.4}Ge_{1.6}(PO_4)_3$ prepared by using a sol–gel method[30] and $Li_{1.5}Al_{0.5}Ge_{1.5}(PO_4)_3$ prepared by using a flame spray technique[31] were found to be 2.8×10^{-4} and 2×10^{-4} S cm^{-1}, respectively, at room temperature. Compared to LAGP prepared by using a solid-state sintering method, glass ceramics prepared by melt quenching demonstrate a denser microstructure with fewer grain boundary effects. The sol–gel and a flame–spray methods allow the preparation of the desired shape and size of the grains of LAGP. However, a flame–spray method requires amorphous LAGP to prepare crystallized $Li_{1.5}Al_{0.5}Ge_{1.5}(PO_4)_3$.

[a] Dr. P. D. Kichambare, T. Howell, Dr. S. Rodrigues
Aerospace Systems Directorate
Air Force Research Laboratory
Wright–Patterson Air Force Base, Ohio 45433-7252 (USA)
E-mail: Padmakar.Kichambare@WPAFB.AF.MIL

[b] T. Howell
GE Aviation
Cincinnati, Ohio 45215 (USA)

Supporting information for this article is available on the WWW under http://dx.doi.org/10.1002/ente.201300139.

Part of a Special Issue on "Energy Storage Materials". To view the complete issue, visit: http://onlinelibrary.wiley.com/doi/10.1002/ente.v2.4/issuetoc

In our previous work,[19–22] $Li_{1.5}Al_{0.5}Ge_{1.5}(PO_4)_3$ was prepared by using the melt-quenching method. Due to safety concerns and the higher calcination temperature needed for melt-quenching and solid-state sintering methods, the sol–gel method was utilized in this work for the synthesis of LAGP. Systematic studies have been performed of the synthesis of LAGP. The sol–gel method was used to synthesize $Li_{1.5}Al_{0.5}Ge_{1.5}(PO_4)_3$ by employing comparatively low-cost $GeCl_2$ as one of the reactants, and the LAGP powder was characterized by various techniques. The influence of the duration of water evaporation during polymerization on the microstructure of LAGP was also examined, and finally, the ionic conductivity and electrocatalytic properties of LAGP were investigated.

Results

The $Li_{1.5}Al_{0.5}Ge_{1.5}(PO_4)_3$ powder was prepared by using a sol–gel process under three different conditions and low-cost $GeCl_2$ as one of the reactants as described in the Experimental Section. Three LAGP specimens were obtained for the following precursor-solution evaporation recipes: 120 °C for 26 h (specimen **1**), 150 °C for 14 h (specimen **2**), and 180 °C for 6 h (specimen **3**).

Microstructure analysis

The X-ray diffraction (XRD) spectra for specimens **1**, **2**, and **3** are shown in Figure 1. The XRD spectra reveal the crystalline phases with the presence of all major peaks of LAGP and impurity peaks of pyrophosphate ($AlPO_4$, shown as *) and Li_2O (shown as ●) in Figure 1. All the major diffraction peaks have been assigned to the Na superionic conductor (NASICON)-type $LiGe_2(PO_4)_3$ structure. It should be noted that in spite of heavy substitution of Al at Ge sites, the diffraction pattern of LAGP matches well with that of $LiGe_2(PO_4)_3$ and this is due to the very similar ionic radii of Ge^{4+} (0.054 nm) and Al^{3+} (0.053 nm). Impurity peaks of the $AlPO_4$ phase at $2\theta = 18°$ and 22° are observed for specimens **1**, **2**, and **3**. For specimen **3**, an additional impurity peak of Li_2O[33] at $2\theta = 20.7°$ is also observed. XRD studies indicate that the duration of water evaporation during the gel formation has an influence on the phase purity of LAGP. It is reported that these impurity phases are mostly segregated at the grain boundaries in LAGP.[32,33]

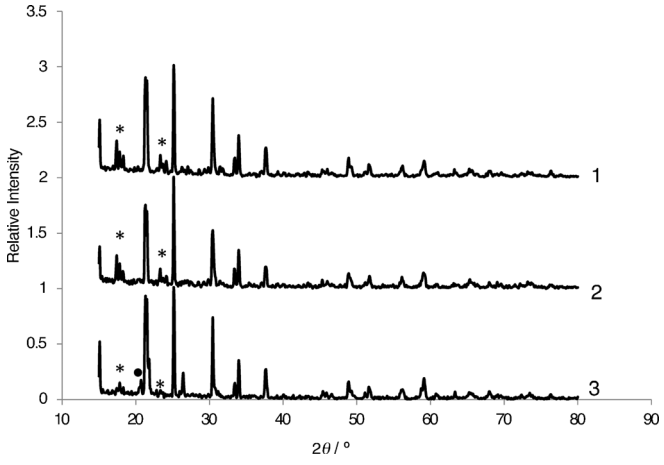

Figure 1. XRD patterns of (1) specimen 1, (2) specimen 2, and (3) specimen 3, for evaporation at 120 °C for 26 h, 150 °C for 14 h, and 180 °C for 6 h, respectively. Impurity peaks of $AlPO_4$ and Li_2O are shown as (*) and (●), respectively.

Shown in Figure 2 a–c are typical SEM images of the LAGP in specimens **1**, **2**, and **3**. It is observed that for water evaporation for 26 h at 120 °C, well-defined crystals are generated with a particle size of approximately 0.6 μm. There is a wide distribution of grain size for LAGP specimens **2** and **3** as depicted in Figure 2 b, c. SEM images (Figure 2 b, c) show well-defined and heterogeneous crystals with particle sizes ranging from 0.7 to 3 μm. Elemental contents in the LAGP specimens were analyzed with energy-dispersive X-ray (EDX) spectroscopy. Al, Ge, O, and P were identified in these specimens. The EDX spectrum shows the presence of the C peak from the conductive carbon tape used during EDX analysis.

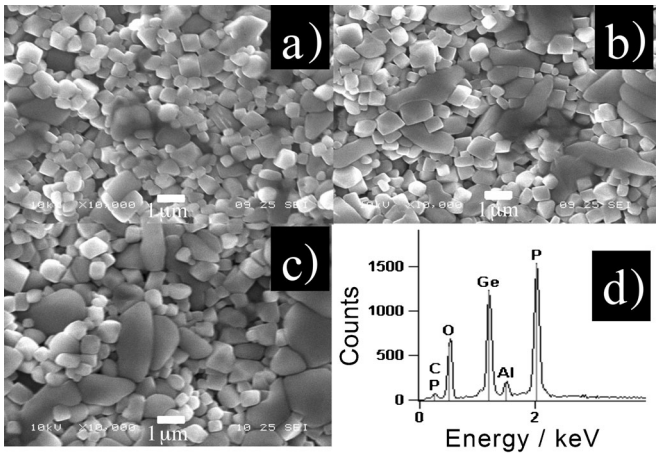

Figure 2. SEM images of LAGP a) specimen **1**, b) specimen **2**, and c) specimen **3** for evaporations at 120 °C for 26 h, 150 °C for 14 h, and 180 °C for 6 h, respectively. The scale bar in SEM images is 1 μm. d) Energy-dispersive X-ray spectroscopy of LAGP specimen **1**.

The Brunauer–Emmett–Teller (BET) nitrogen adsorption–desorption isotherms of specimens **1**, **2**, and **3** were obtained. Shown in Figure 3 a is a typical nitrogen adsorption isotherm for specimen 1. BET surface area and pore volume values of specimens **1**, **2**, and **3** were determined and are summarized

Table 1. Physical and electrical properties of LAGP electrolytes.

LAGP Electrolytes	BET surface area [$m^2 g^{-1}$]	Pore volume [$cm^3 g^{-1}$]	Ionic conductivity [$S cm^{-1}$] at room temp.	Activation energy [eV]
specimen **1**	4.28	0.015	1.03×10^{-4}	0.46
specimen **2**	3.91	0.012	8.33×10^{-5}	0.42
specimen **3**	2.12	0.006	8.88×10^{-5}	0.48

The precursor solution was evaporated for specimen **1** at 120 °C for 26 h, specimen **2** at 150 °C for 14 h, and specimen **3** 180 °C for 6 h.

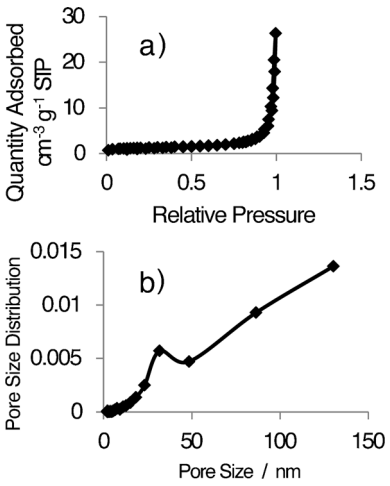

Figure 3. a) N_2 adsorption–desorption isotherms of specimen **1** and b) pore size distributions of specimen **1** as calculated by using the BJH method.

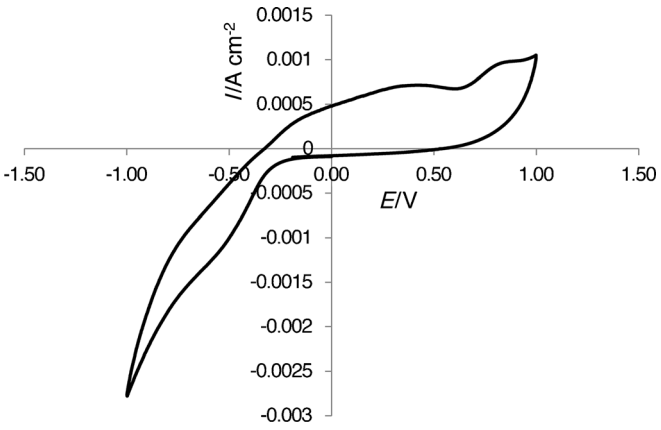

Figure 4. Cyclic voltammogram of specimen **1** in oxygen-saturated aqueous KOH (0.1 M) at 25 °C with a scan rate of 5 mV min^{-1}.

in Table 1. Significant nitrogen uptake above the relative pressure ratio of 0.90 has been observed in the BET isotherm (Figure 3 a) and this is due to the condensation of nitrogen in the porous structure of the LAGP. The pore size distributions for the LAGP specimens are derived by using the Barrett–Joyner–Halenda (BJH) method. Figure 3 b shows the pore size distribution curve for specimen **1** is centered at a pore diameter of 30 nm.

Electrocatalytic performance for oxygen reduction and evolution reactions

The electrocatalytic ability of specimens **1**, **2**, and **3** were evaluated by cyclic voltammetry (CV). These CV measurements were performed in an oxygen-saturated aqueous solution of KOH (0.1 M). Shown in Figure 4 is a typical CV curve of specimen **1** with reference to the saturated calomel electrode (SCE). The oxygen reduction reaction (ORR) and oxygen evolution reaction (OER) potentials for specimen **1** were found at approximately −0.50 V and 0.80 V (vs SCE), respectively. No electrocatalytic activity was observed if the electrolyte was saturated with nitrogen. The cathodic and anodic peak current intensities for specimen **1** are 1.2 and 1 mA cm^{-2}, respectively. Similar ORR and OER activities were observed for specimens **2** and **3**. The impurity phases present in the LAGP did not affect the ORR and OER activities.

All of these ions—superoxide (O_2^-), peroxide (O^-), and oxide (O^{2-})—can be produced in the oxygen-reduction process specifically as the CV measurements are being performed in liquid electrolytes.[34–36] There are asymmetries in the peak locations and intensities that indicate a measure of irreversibility in the reaction. The criteria for reversibility of a reaction from the CV data are often expressed in terms of the ratio of cathodic (i_{pc}) and anodic (i_{pa}) peak current densities and the corresponding potential difference Δ ($E_{pc}-E_{pa}$) = (59/n) mV, in which E_{pc}, E_{pa}, and n are the cathodic potential, anodic potential, and number of electrons participating in the reaction, respectively.[37] The i_{pc}/i_{pa} ratio and Δ ($E_{pc}-E_{pa}$) for specimen **1** are 1.09 and 1.29 V, respectively. The irreversibility of the reaction may stem from a kinetic hindrance to the transport of O_2 and Li^+ and an asymmetric activation energy for the involved reactions. This indicates that the LAGP specimens are efficient electrocatalysts for ORR and OER in lithium–oxygen batteries.

Impedance spectroscopy and ionic conductivity

Representative Nyquist impedance plots of LAGP specimens **1**, **2**, and **3** are depicted in Figure 5. Impedance spectra were collected to analyze the frequency response of LAGP specimens over wide temperature range, from −40 °C to 110 °C. The plots were normalized to the geometrical factor t/A for each specimen, in which t and A are the thickness and area of the LAGP pellet, respectively. The impedance spectra of the LAGP specimens show a compressed semicircle that corresponds to ion conduction in the bulk of the

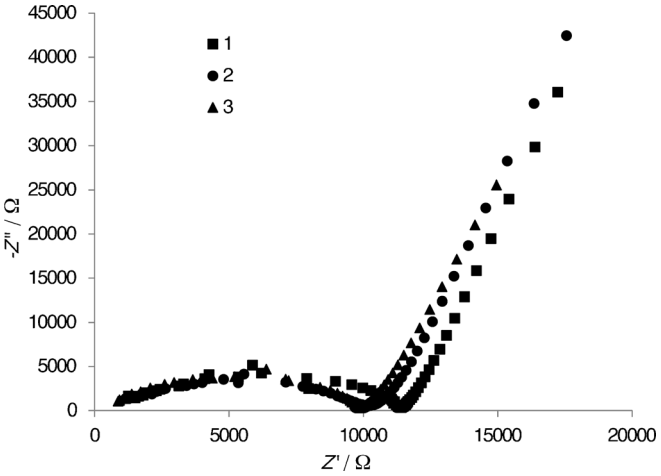

Figure 5. Nyquist Impedance plots of LAGP specimens **1** (■), **2** (●), and **3** (▲) at room temperature.

specimens and the tail relates to electrode polarization. The semicircle demonstrates that LAGP behaves as an electrolyte resistance in parallel with an interelectrode capacitance. The intersection of the semicircle with the real axis shows a high conductivity of 1.03×10^{-4} S cm^{-1} (specimen **1**) that points to fast lithium-ion conduction in highly crystalline LAGP. The disappearance of the bulk impedance semicircle at higher temperature in the impedance profile is observed (Figure S1 in Supporting Information) and is due to the very low resistance of LAGP which typically responds at very high frequencies. These results are consistent with those reported for glass ceramics with NASICON-type structures.[31,38] The conducting properties of these ionic conductors depend on the crystalline phase and the tunnel size for lithium-ion migration. The ionic conductivities of these LAGP specimens are comparable to those of other lithium ionic conductors.[27,31,39]

The Arrhenius plots of the conductivities for specimens **1**, **2**, and **3** are shown in Figure 6 and they indicate that the

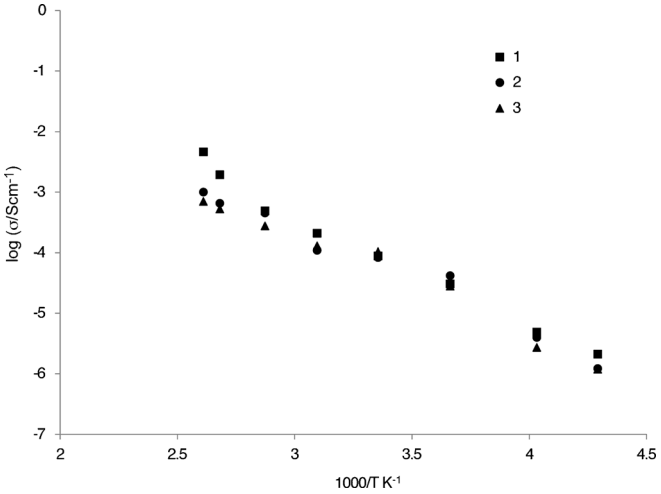

Figure 6. Arrhenius plots of the ionic conductivity of LAGP specimens **1** (■), **2** (●), and **3** (▲).

ionic conductivity of LAGP increase with temperature. The ionic conductivities for all LAGP specimens were calculated from the bulk resistance of LAGP derived from the Nyquist plots. The conductivity data were found to fit well to the Arrhenius equation. The activation energies for specimens **1**, **2**, and **3**, derived from the slopes of the Arrhenius plots, were found to be 0.46, 0.42, 0.48 eV, respectively. The small variation in activation energy for specimens **1**, **2**, and **3** may be due to the increase in grain size of LAGP as observed in Figure 2. There is a significant increase in conductivity on the order of 10^{-3} S cm^{-1} at higher temperatures as illustrated in Figure 6. The ionic conductivity of LAGP specimens at higher temperatures is comparable to that of ionic liquid electrolytes at room temperature.[40]

Application to solid-state lithium–oxygen cell

As a first step in realizing the application of sol–gel-derived LAGP as electrolyte, a solid-state lithium–oxygen test cell was fabricated similar to the one reported in our previous work.[22] Figure S2 shows a portion of discharge–charge behavior of the lithium–oxygen cell with sol–gel-derived LAGP as electrolyte with a low discharge current of 0.05 mA at 75 °C. In this test cell, the cathode was nitrogen-doped carbon with 5 wt % LAGP and the anode was lithium metal. It is apparent from the Figure S2 that the cell is reversibly charged and discharged at charge/discharge currents of 0.05 mA.

Discussion

In this study, synthesis of the solid electrolyte LAGP with uniform particle size for lithium–oxygen batteries was demonstrated by using a sol–gel process. The influence of the duration of water evaporation during polymerization on the microstructure of LAGP was further examined. The drying time for sol–gel plays a direct role in the microstructure of the final material due to the distribution of pores throughout the gel. From the BET results it was observed that the surface area of the particles increased with long evaporation times. The longer evaporation time also leads to more uniform and smaller particle sizes as demonstrated in the SEM images. Table 1 indicates that specimen **1** exhibits higher conductivity than specimens **2** and **3**. The higher conductivity of specimen **1** is attributed to the uniform particle size. XRD studies clearly demonstrate the presence of a dominant crystalline phase of LAGP along with a small impurity phase of $AlPO_4$. This impurity phase may have been formed due to insufficient mixing of Ge with the Al source. Using a longer mixing time may help reduce the impurity phase of $AlPO_4$.

It is observed from Nyquist impedance plots that the apparent diameter of the semicircle for specimens **2** and **3** is smaller than that of specimen **1**. The larger diameter for specimen **1** is probably due to a higher concentration of impurity phase in the intergranular region that influenced lithium-ion conduction. The Arrhenius plots (Figure 6) of the specimens are nearly linear and that is attributed to the presence of impurity $AlPO_4$ in the LAGP solid electrolyte.[41] This indicates that the impurity phase has an influence on the conductivity of LAGP.

CV measurements revealed electrocatalytic activity of LAGP towards the oxygen reduction and oxygen evolution reactions that correlates with the number of available catalytic sites and adsorption affinity for oxygen on LAGP. It is foreseeable that the ionic conductivity and electrocatalytic activity of the LAGP solid electrolyte can be further improved through chemical manipulations.

Conclusions

LAGP was prepared by using a sol–gel process under three different precursor-solution evaporation conditions: 120 °C

for 26 h (specimen **1**), 150 °C for 14 h (specimen **2**), and 180 °C for 6 h (specimen **3**). LAGP was found to be dominant crystalline phase. Small amounts of pyrophosphate ($AlPO_4$) and Li_2O as impurity phases were detected. The highest room-temperature ionic conductivity of LAGP was found to be 1.03×10^{-4} S cm^{-1}. LAGP prepared by sol–gel process also showed electrocatalytic activity towards the ORR and OER. The preliminary electrochemical studies on sol–gel-derived LAGP indicate that it acts as a electrolyte in lithium–oxygen cells. These studies suggest that LAGP is a promising solid electrolyte and electrocatalyst for all-solid-state lithium–oxygen batteries.

Experimental Section

Materials

Analytical grade $LiNO_3$ (Sigma–Aldrich), $NH_4H_2PO_4$ (Acros Organics), $Al(NO_3)_3$ (Sigma–Aldrich), and $GeCl_2$ (Sigma–Aldrich) were used as received.

Synthesis of LAGP

In a typical sol–gel synthesis of LAGP, the precursor nitrates of analytical grade $LiNO_3$, $NH_4H_2PO_4$, and $Al(NO_3)_3$ were dissolved in deionized water to generate stock solutions. For a Ge stock solution, $GeCl_2$ was dissolved in ethanol inside a dry box. Stoichiometric amounts of nitrate solutions were placed into a glass beaker (2 L). Ethylene glycol (Sigma–Aldrich) and citric acid (Alfa Aesar) (1:1 molar ratio) were added to the nitrate solution as a chelating agent to obtain a homogeneous solution. This homogeneous solution was kept at 120 °C (specimen **1**) for 26 h to allow the evaporation of water and to achieve a dry powder in one case. In the other two cases, the homogeneous solutions were maintained at 150 °C (specimen **2**) and 180 °C (specimen **3**) for 14 h for 6 h, respectively. The resulting dry powder was pyrolyzed at 500 °C to release the volatile compounds and further calcined in a high-purity alumina crucible at 800 °C for 5 h with a heating rate of 1 °C min^{-1} at ambient conditions (in air). The resulting powder was then cooled and ground using an agate mortar and further reground for 1 h, by using high-energy ball milling (SPEX SamplePrep 8000M Mill) to obtain a fine powder. This fine powder was sintered in an alumina crucible at 900 °C for 6 h to achieve a well-crystallized LAGP powder.

Measurements

Morphologies of LAGP specimens **1**, **2**, and **3** were examined by using scanning electron microscopy (SEM). The elemental content in the LAGP specimens was analyzed using energy-dispersive X-ray (EDX) spectroscopy. X-ray diffraction (XRD) data for the LAGP specimens were obtained using a Bruker D8 Discover diffractometer operated at 40 kV and 40 mA with $Cu_{K\alpha}$ over the 2θ range of 15 to 80° in steps of 0.05°. The Brunauer–Emmett–Teller (BET) surface areas of the LAGP specimens were obtained by using a nitrogen sorption instrument (Micromeritics ASAP 2020). The LAGP specimens were degassed for 4 h at 250 °C under vacuum before surface area measurements. Cyclic voltammetry (CV) measurements were performed in a standard three-electrode cell configuration with oxygen-saturated aqueous KOH (0.1 M) as the electrolyte by using a VersaStat 4 electrochemical analyzer. Pastes consisting of the LAGP specimen and Nafion (tetrafluoroethylene-based fluoropolymer copolymer) solution were prepared and spread on graphite, which was used as the working electrode. A Pt wire was used as the counter electrode and a saturated calomel electrode (SCE) electrode was used as the reference electrode. Electrochemical impedance spectroscopy (EIS) measurements on LAGP specimens were conducted over a frequency range of 1 Hz to 10^6 Hz by using a VersaSTAT 4 (Princeton Applied Research) electrochemical workstation. For impedance measurements, pellets of LAGP specimens (0.8 mm thickness, 1.2 cm diameter) were prepared and heated at 1 °C min^{-1} up to 850 °C and sintered at that temperature for 24 h before cooling down to room temperature at a rate of 2 °C min^{-1}. Dense pellets with smooth surfaces were obtained. A gold coating (0.5 mm thickness) was sputtered on both sides of the pellets to achieve good electrical contact. Charge–discharge measurements of the solid-state lithium–oxygen cell were performed in a galvanostatic mode under an oxygen atmosphere.

Acknowledgements

This research was supported by the Air Force Research Laboratory, Wright–Patterson Air Force Base, Ohio.

Keywords: LAGP · lithium–oxygen batteries · solid electrolytes · sol–gel processing · superionic conductors

[1] P. G. Bruce, S. A. Freunberger, L. J. Hardwick, J. M. Tarascon, *Nat. Mater.* **2012**, *11*, 19–29.
[2] H. G. Jung, J. Hassoun, J. B. Park, Y. K. Sun, B. Scrosati, *Nat. Chem.* **2012**, *4*, 579–585.
[3] S. H. Oh, R. Black, E. Pomerantseva, J. H. Lee, L. F. Nazar, *Nat. Chem.* **2012**, *4*, 1004–1010.
[4] Y. C. Lu, B. M. Gallant, D. G. Kwabi, J. R. Harding, R. R. Mitchell, M. S. Whittingham, Y. Shao-Horn, *Energy Environ. Sci.* **2013**, *6*, 750–768.
[5] Z. Peng, S. A. Freunberger, Y. Chen, P. G. Bruce, *Science* **2012**, *337*, 563–566.
[6] K. M. Abraham, Z. Jiang, *J. Electrochem. Soc.* **1996**, *143*, 1–5.
[7] G. M. Veith, N. J. Dudney, J. Howe, J. Nanda, *J. Phys. Chem. C* **2011**, *115*, 14325–14333.
[8] H.-G. Jung, H.-S. Kim, J.-B. Park, I.-H. Oh, J. Hassoun, C. S. Yoon, B. Scrosati, Y.-K. Sun, *Nano Lett.* **2012**, *12*, 4333–4335.
[9] S. A. Freunberger, Y. Chen, Z. Peng, J. M. Griffin, L. J. Hardwick, F. Barde, P. Novak, P. G. Bruce, *J. Am. Chem. Soc.* **2011**, *133*, 8040–8047.
[10] H. Wang, Y. Yang, Y. Liang, G. Zheng, Y. Li, Y. Cui, H. Dai, *Energy Environ. Sci.* **2012**, *5*, 7931–7935.
[11] B. Sun, P. Munroe, G. X. Wang, *Sci. Rep.* **2013**, *3*, 2247.
[12] E. Yilmaz, C. Yogi, K. Yamanaka, T. Ohta, H. R. Byon, *Nano Lett.* **2013**, *13*, 4679–4684.
[13] Y. Shao, S. Park, J. Xiao, J. G. Zhang, Y. Wang, J. Liu, *ACS Catal.* **2012**, *2*, 844–857.
[14] J. Wang, Y. Li, X. Sun, *Nano Energy* **2013**, *2*, 443–467.
[15] J. Christensen, P. Albertus, R. S. Sanchez-Carrera, T. Lohmann, B. Kopzinsky, R. Liedtke, J. Ahmed, A. Kojic, *J. Electrochem. Soc.* **2012**, *159*, R1–R30.
[16] G. Girishkumar, B. McCloskey, A. C. Luntz, S. Swanson, W. Wilcke, *J. Phys. Chem. Lett.* **2010**, *1*, 2193–2203.
[17] N. Kamaya, K. Homma, Y. Yamakawa, M. Hirayama, R. Kanno, M. Yonemura, T. Kamiyama, Y. Kato, S. Hama, K. Kawamoto, A. Mitsui, *Nat. Mater.* **2011**, *10*, 682–686.
[18] Y. Sun, *Nano Energy* **2013**, *2*, 801–816.

[19] B. Kumar, J. Kumar, R. Leese, J. P. Fellner, S. J. Rodrigues, K. M. Abraham, *J. Electrochem. Soc.* **2010**, *157*, A50–A54.
[20] P. Kichambare, J. Kumar, S. Rodrigues, B. Kumar, *J. Power Sources* **2011**, *196*, 3310–3316.
[21] P. Kichambare, S. Rodrigues, J. Kumar, *ACS Appl. Mater. Interfaces* **2012**, *4*, 49–52.
[22] P. Kichambare, S. Rodrigues, *Energy Technol.* **2013**, *1*, 209–211.
[23] B. Key, D. J. Schroeder, B. J. Ingram, J. T. Vaughey, *Chem. Mater.* **2012**, *24*, 287–293.
[24] a) F. Li, H. Kitaura, H. Zhou, *Energy Environ. Sci.* **2013**, *6*, 2302–2311; b) T. Zhang, H. Zhou, *Nat. Commun.* **2013**, *4*, 1817.
[25] B. Kumar, P. Kichambare, S. Rodrigues, J. Kumar, R. G. Keil, *Electrochem. Solid-State Lett.* **2011**, *14*, A97–A99.
[26] X. Xu, Z. Wen, X. Wu, X. Yang, Z. Gu, *J. Am. Ceram. Soc.* **2007**, *90*, 2802–2806.
[27] J. Fu, *Solid State Ionics* **1997**, *104*, 191–194.
[28] J. S. Thokchom, N. Gupta, B. Kumar, *J. Electrochem. Soc.* **2008**, *155*, A915–A920.
[29] C. J. Leo, G. V. Subba Rao, B. V. R. Chowdari, *Solid State Ionics* **2003**, *159*, 357–367.
[30] M. Zhang, K. Takahashi, N. Imanishi, Y. Takeda, O. Yamamoto, B. Chi, J. Pu, J. Li, *J. Electrochem. Soc.* **2012**, *159*, A1114–A1119.
[31] C. R. Mariappan, C. Yada, F. Rosciano, B. Roling, *J. Power Sources* **2011**, *196*, 6456–6464.
[32] J. S. Thokchom, B. Kumar, *J. Power Sources* **2010**, *195*, 2870–2876.
[33] J. S. Thokchom, B. Kumar, *J. Power Sources* **2008**, *185*, 480–485.
[34] C. O. Laoire, S. Mukerjee, K. M. Abraham, E. J. Plichta, M. A. Hendrickson, *J. Phys. Chem. C* **2009**, *113*, 20127–20134.
[35] Y. Liang, Y. Li, H. Wang, H. Dai, *J. Am. Chem. Soc.* **2013**, *135*, 2013–2036.
[36] Y. Zhao, L. Xu, L. Mai, C. Han, Q. An, X. Xu, X. Liu, Q. Zhang, *Proc. Natl. Acad. Sci. USA* **2012**, *109*, 19569–19574.
[37] A. J. Bard, L. R. Faulkner, *Electrochemical Methods: Fundamentals and Applications, 2nd ed.*, Wiley, New York, **2001**.
[38] C. R. Mariappan, M. Gellert, C. Yada, F. Rosciano, B. Roling, *Electrochem. Commun.* **2012**, *14*, 25–28.
[39] X. Xu, Z. Wen, Z. Gu, X. Xu, Z. Lin, *Solid State Ionics* **2004**, *171*, 207–213.
[40] a) M. A. Taige, D. Hilbert, T. J. S. Schubert, *Z. Phys. Chem. (Muenchen Ger.)* **2012**, *226*, 129–139; b) G. B. Appetecchi, G. T. Kim, M. Montanino, F. Alessandrini, S. Passerini, *J. Power Sources* **2011**, *196*, 6703–6709.
[41] M. Kotobuki, M. Koishi, *Ceram. Int.* **2013**, *39*, 4645–4649.

Received: October 11, 2013
Revised: December 23, 2013
Published online on March 12, 2014